Numerical Investigation of the mechanisms of Ultrasound-modulated Bioluminescence Tomography

Qimei Zhang[1], Melissa L Mather[1, 2], Stephen P Morgan[1]

[1]Applied Optics Group, Electrical Systems and Optics Research Division, Faculty of Engineering, University of Nottingham, UK

[2]Institute of Biophysics, Imaging and Optical Sciences, Faculty of Engineering, University of Nottingham, UK

ABSTRACT

Objective: A hybrid imaging technique, Ultrasound Modulated Luminescence Tomography, that uses ultrasound to modulate diffusely propagating light has been shown to improve the spatial resolution of optical images. This paper is to investigate the underlying modulation mechanisms and the feasibility of applying this technique to improve the spatial resolution of bioluminescence tomography. **Methods**: Ultrasound Modulated Bioluminescence Tomography was studied numerically to identify the dominance of four factors (reduced optical scattering coefficient, optical absorption coefficient, refractive index, and luciferase concentration) on the depth of light modulation. In practice, an open source finite element method tool for simulation of diffusely propagating light, Near Infrared Fluorescence and Spectral Tomography, was modified to incorporate the effects of ultrasound modulation. The signal-to-noise ratios of detected modulated bioluminescent emissions are calculated using the optical and physical properties of a mouse model. **Results**: The modulation depth of the bioluminescent emission affected by the US induced variation of local concentration of the light emitting enzyme luciferase were at least two orders of magnitude greater than that caused by variations in the other factors. For surface radiances above approximately 10^7 photons/s/cm^2/sr the corresponding SNRs are detectable with the current detector technologies. **Conclusion**: The dominant effect in generation of ultrasound modulated bioluminescence is ultrasound induced variation in luciferase concentration. The SNR analysis results confirm the feasibility of applying Ultrasound Modulated Bioluminescence Tomography in preclinical imaging of mice. **Significance**: The simulation model developed suggests ultrasound modulated bioluminescence tomography is a potential technique to improve the spatial resolution of bioluminescence tomography.

Bioluminescence tomography is an optical molecular imaging method that can be used to assess the functional and pathological status of biological tissue *in vivo*. The achievable spatial resolution is severely limited by the dominance of optical scattering of the bioluminescent emission. A hybrid imaging technique, Ultrasound Modulated Optical Tomography (USMOT), that uses ultrasound to

modulate diffusely propagating light has been shown to improve the spatial resolution of optical images. Here the mechanisms of ultrasound modulation and the feasibility of applying USMOT to improve the spatial resolution of bioluminescence tomography are investigated. Ultrasound Modulated Bioluminescence Tomography (USMBLT) was studied numerically to identify the dominance of four factors (reduced optical scattering coefficient, optical absorption coefficient, refractive index, and luciferase concentration) on the depth of light modulation. In practice, an open source finite element method tool for simulation of diffusely propagating light, Near Infrared Fluorescence and Spectral Tomography (NIRFAST), was modified to incorporate the effects of ultrasound modulation. Simulation results show the modulation of the bioluminescent emission is significantly affected by the local concentration of the light emitting enzyme luciferase in comparison to the reduced scattering coefficient, absorption coefficient and refractive index. The feasibility of applying USMBLT in pre-clinical imaging was demonstrated by comparing the calculated signal-to-noise ratios of detected modulated bioluminescent emissions using the optical and physical properties of a mouse model with that of the limits of current detector technologies.

Keywords: ultrasound modulated optical tomography, bioluminescence tomography, Finite Element Method, NIRFAST.

1 INTRODUCTION

Bioluminescence tomography (BLT) is based on the generation of visible light by a living organism resulting from an enzymatic reaction [1]. It is a sensitive technique that can be used to monitor cellular events in living tissues [2]. Advantageously BLT is characterised by extremely low background signals, short acquisition times (seconds to minutes) and high signal-to-noise ratios (SNRs) [3]. Moreover, due to its non-invasive nature and capability to enable longitudinal studies it is expected to have a significant impact on the implementation of strategies to reduce the number of animals used in pre-clinical imaging within the Principles of Humane Experimental Techniques. The achievable spatial resolution of images in BLT is, however, severely limited by the dominance of optical scattering in bioluminescent photon propagation in tissue. Strategies have been developed to help overcome the low resolution of BLT including the use of spectrally resolved BLT as a means to estimate the depth of an object based on the wavelength dependence of attenuation in tissue [4] and dual-modality molecular imaging techniques that co-register BLT images with those from other modalities such as magnetic resonance imaging (MRI) or positron emission tomography (PET) [2].

Alternative approaches to improve spatial resolution when diffuse light dominates are photo-acoustic tomography (PAT) [5] and ultrasound modulated optical tomography (USMOT) [6]. These

are hybrid approaches which combine the advantages of ultrasonic and optical imaging techniques. In PAT, ultrasound (US) waves are excited by irradiating tissue with nanosecond scale pulses of light. Optical absorption by specific tissue chromophores (e.g. haemoglobin, melanin, flavins) produces a small temperature rise (less than 0.1 ^{o}C) that generates a broadband, low amplitude (less than 10 kPa) acoustic emission. Here image formation is based on the acoustic signals radiating from the surface of the sample, which are scattered much less in tissue than light. This approach, however, is not applicable to BLT as there is no pulsed light source present to generate acoustic waves. In USMOT, light illuminates the tissue and US is used to modulate its optical properties (absorption coefficient, reduced scattering coefficient and refractive index) at a rate corresponding to the US frequency which subsequently produces frequency modulated light. By spatially confining the US beam, images based on the optical properties of tissue localised within the US field can be obtained via detection of the modulated light.

Conventionally temporally coherent light has been used in USMOT. Recently, however, ultrasound modulated fluorescence tomography (USMFT) [7-9] was performed which demonstrates the feasibility of USMOT with short coherence length light sources and hence its potential application in BLT. A current difficulty of USMOT using low coherence sources is the weak modulation of light it produces, quantified by measurement of the modulation depth which is defined as the ratio between modulated light intensity (AC signal) and unmodulated light intensity (DC signal) [10]. The modulation depth for USMFT is of the order of 10^{-4} to 10^{-6} [11] as compared to 10^{-2} that is achieved using a laser source. In relation to imaging, the use of low coherent light sources produces modulated optical signals with low SNRs and image quality is limited by the capabilities of the signal detection device.

Unlike fluorescence, bio- (or chemi-) luminescence does not require the use of excitation light to produce emission. In relation to imaging this eliminates the possibility of background signals being produced by the excitation light and any light generated by autofluorescence, and hence improves the achievable SNRs. This was recently demonstrated in a study that imaged a tissue phantom containing a chemi-luminescent material using Ultrasound Modulated Luminescence Tomography (USMLT) [12]. Here the SNR was found to be 80 and the image lateral resolution was 3 mm at a depth of 7 mm within a tissue phantom with a scattering coefficient of 30 cm^{-1}. This represents a 3.5 times improvement in spatial resolution compared to the conventional unmodulated optical tomography. More recently a method to reconstruct the density of a luminescent source in a highly scattering medium was presented based on the solution to a hybrid inverse source problem for the diffusion equation [13]. Using this approach the spatial resolution in reconstructed images was improved by a factor of 10 as compared to that in conventional BLT. These studies provide support

to the hypothesis that US modulation techniques could be applied to improve the spatial resolution of BLT. Both the inverse problems of USMLT and BLT are to determine the source density distribution in the volume from boundary measurements of multiple scattered light based on radiative transport. Therefore it can be expected that the existing BLT reconstruction algorithms can be modified to be applied in the reconstruction of USMLT through coupling between US and light in terms of quantities that are changed by US pressure. Since the number of measurements can be dramatically increased by scanning US field and detecting US modulated luminescence signal, USMLT should be able to substantially help overcome the ill-posedness of the inverse problem.

In the present study, the mechanisms of Ultrasound Modulated Bioluminescence Tomography (USMBLT) are first studied numerically to identify the dominance of four factors (reduced optical scattering coefficient, optical absorption coefficient, refractive index, and concentration of the bioluminescent target (luciferase)) on the strength of light modulation. In practice, an open source finite element method (FEM) tool for simulation of diffusely propagating light, Near Infrared Fluorescence and Spectral Tomography (NIRFAST), which simulates light propagation in biological tissue based on the finite element method (FEM), is modified to incorporate the effects of ultrasound modulation. The feasibility of applying USMBLT to imaging pre-clinical models is also investigated by calculating the SNR of USMBLT using the optical and physical properties of mice reported in the literature. Finally strategies to improve the SNR are discussed as well as the future prospects of USMBLT.

2 METHODS

2.1 Forward light modelling

The fluence rate of the US modulated bioluminescence signal from a source located inside a tissue sample was calculated through modification of the open source model of light transport NIRFAST. In this case the fluence rate (W/mm^2) of bioluminescent photons detected at the surface of a tissue sample can be calculated by calling the forward model in NIRFAST, which solves the following diffusion approximation of the radiative transport equation in the frequency domain [14],

$$-\nabla \cdot k(r)\nabla\Phi(r,w) + \left(\mu_a(r) + \frac{iw}{c_m(r)}\right)\Phi(r,w) = q_0(r,w), \quad (1)$$

where $k(r) = 1/3(\mu_a(r) + \mu_s'(r))$ is the diffusion coefficient, $\mu_a(r)$ is the absorption coefficient, $\mu_s'(r)$ is the reduced scattering coefficient, $\Phi(r,w)$ is the photon fluence rate at the position r, w is the modulation frequency, $c_m(r) = c_0/n(r)$ is the speed of light in the medium, c_0 is the speed of light in vacuum, $n(r)$ is the refractive index, and $q_0(r,w)$ is an isotropic source term.

To solve the diffusion approximation by FEM, a tetrahedral mesh for the volume of the tissue sample was generated containing an internal bioluminescence source and boundary data [15]. The mesh was comprised of a number of elements joined at vertex nodes. The optical properties of the sample were assigned to the mesh directly by using the Graphic User Interface (GUI) of NIRFAST. The simulations in this paper are based on equation (1).

2.2 Ultrasound modulation of sample optical properties and luciferase concentration

In order to investigate the underlying mechanisms of USMBLT the NIRFAST model was modified to account for the US induced temporal oscillation of the sample optical properties (reduced scattering coefficient, absorption coefficient, and refractive index). Changes in the bioluminescence intensity due to the oscillation of luciferase concentration were also taken into account.

A starting point for establishing a framework to simulate USMBLT is consideration of the time dependent US field by defining the term *US*(*t*):

$$US(t) = Asin\left(\vec{k} \cdot \vec{r} - wt\right), \tag{2}$$

where $A = \frac{P_0}{w_{us}\rho_0 v_a}$ [16] is the particle displacement amplitude, which is a function of the US pressure (P_0), the US angular frequency (w_{us}), the mass density of the sample (ρ_0) and the acoustic velocity in the sample (v_a). Of note is that P_0 is the pressure at the fundamental frequency at the US focal zone.

With reference to the literature [17] expressions for the US induced variation in sample optical parameters can be obtained:

$$\Delta n = n_0 \eta k US(t), \tag{3a}$$

$$\Delta \mu_s{}' = \mu_{s0}{}'[1 + 0.37\eta] k US(t), \tag{3b}$$

$$\Delta \mu_a = \mu_{a0} k US(t), \tag{3c}$$

where Δn, $\Delta \mu_s{}'$ and $\Delta \mu_a$ are the changes in the refractive index, reduced scattering coefficient and absorption coefficient respectively. Here $n_0, \mu_{s0}{}', \mu_{a0}$ are the corresponding equilibrium refractive index, reduced scattering coefficient, and absorption coefficient in the absence of US modulation. $\vec{k}$ is the wave vector, $k = \frac{2\pi}{\lambda_{us}}$ is the relative scalar, λ_{us} is the US wavelength, and $\vec{r}$ represents the

spatial position. η is the elasto-optic coefficient which is related to the adiabatic piezooptical coefficient of the sample $\partial n/\partial p$, ρ_0 and v_a such that $\eta = (\partial n/\partial p)\,\rho_0 v_a^2$ [18].

The next parameter for which the effects of US are considered is the bioluminescence intensity (photons/s/L) from the bioluminescence source. In the unmodulated case the bioluminescence intensity generated from an ATP/luciferin-luciferase solution can be expressed as [19]:

$$q_0 = QYk_{cat}C_0, \tag{4}$$

where *QY* (photons/molecule) is the quantum yield of bioluminescence reactions and is defined as the efficiency of the production of a photon from a single reactant molecule. k_{cat} (s^{-1}) is the catalytic constant, which represents the turnover number that indicates the maximum number of molecules of substrate that an enzyme can convert to product per catalytic site per second [19]. C_0 is the concentration (molecule/L) of the enzyme at the site of interest in the tissue (active luciferase).

The enzyme concentration under the interaction of an US field can be written as [20]

$$C_1 = C_0\big(1 + \beta_a' P(\mathrm{r},\mathrm{t})\big), \tag{5}$$

where $\beta_a' = \frac{k}{\rho_0 v_a w} \cdot \frac{1+\hat{\varepsilon}-i\left[\hat{\varepsilon}+\frac{2}{3}\hat{\varepsilon}^2\right]}{1+\hat{\varepsilon}-i\left[\hat{\varepsilon}+\frac{4}{9}\left(\rho+\frac{1}{2}\right)\hat{\varepsilon}^2\right]} + \beta_a$, $\hat{\varepsilon} = \sqrt{wa^2/2\gamma}$, a is the radius of the enzyme molecule, γ is fluid kinematic viscosity, $\rho = \frac{\rho_l}{\rho_0}$, ρ_l is the substrate density and can be obtained from the molecule radius and the molar mass, $\beta_a = 1/K$ is the compressibility of tissue, $K=v_a^2\rho_0$ is the bulk modulus, and $P(r,t)$ is the acoustic pressure. Replacing C_0 in eq.(6) with C_1 in eq.(7), the bioluminescence intensity under the interaction of the US field is expressed as:

$$q = QYk_{cat}C_0\big(1 + \beta_a' P(r,t)\big). \tag{8}$$

The relative variation of the bioluminescence intensity can then be expressed from eq. (8) and eq. (6) as:

$$\frac{\Delta q}{q_0} = \frac{|q-q_0|}{q_0} = \beta_a' P(r,t). \tag{10}$$

3 SIMULATIONS

3.1 Simulation methods

The NIRFAST software tool was used to assign optical properties to nodes in the three dimensional (3D) mesh representing a tissue phantom. This assignment involved identification of nodes that lay inside a specified US field, as calculated using Eq.(2), by comparing the spatial co-ordinates of the

individual nodes to that of the US field. Eq. (3) was then used to calculate the temporal and spatial variation of the tissue optical properties in this field. Nodes outside the US field were assigned equilibrium properties of the tissue being modelled. It should be noted that the optical parameters in eq. (1) are time-independent. In this paper the temporal change of the optical properties are simulated by calculating the bioluminescence fluence rates separately at 24 phases within a period and then connecting all these fluence rates in sequence (as shown later in Fig. 6.).

The spatial co-ordinates of the bioluminescence source were next specified. In practice, the region of the bioluminescence source was divided into several layers along the direction of US propagation, each with an allocated pressure. The bioluminescence intensity by each layer was then determined using Eq. (6). Finally the modulation depth was calculated using:

$$m = \frac{|F_{US} - F|}{F}, \tag{6}$$

While F_{US} and F are the bioluminescence fluence rates detected at the surface in the presence and absence of US respectively.

3.2 SNR analysis of *in vivo* detection

Calculations were carried out to predict the SNR that could be achieved in the *in vivo* application of USMBLT. These calculations were based on use of parameters relating to realistic experimental configurations. Here the detection system was considered to consist of a PMT, transimpedance amplifier and lock-in amplifier (LIA). The SNR for such a system can be expressed as:

$$\text{SNR} = \frac{P_m}{P_n}, \tag{7}$$

where P_m is the power of the detected modulated signal, $P_n = P_{ns} + P_{dc} + P_a$ is the total noise power, with P_{ns}, P_{dc} and P_a relating to the noise arising from the bioluminescence light (modulated signal and unmodulated signal), dark current and ambient light level respectively.

Calculation of the SNR also requires knowledge of the output voltage of the transimpedance amplifier. The output relating to the expression of bioluminescence modulated by US with a frequency of f_{US} is:

$$v_{AC} = V_{AC} \sin(2\pi f_{US} t) \tag{8}$$

$$V_{AC} = 2\pi S L_{AC} h f E_{Ano} R M, \tag{9}$$

where S is the effective area of the PMT, L_{AC} ($\text{photons/s/cm}^2\text{/sr}$) is the modulated surface radiance, h is Planck's constant, $f = c/\lambda$ is the light frequency, and λ is the light wavelength. E_{Ano} is

the anode radiance sensitivity of the PMT in the bioluminescence wavelength, R and M are the input impedance and gain of the transimpedance amplifier respectively.

Thus the power of the optical modulated signal can be expressed by:

$$P_m = \frac{V_{AC}^2}{2}. \tag{10}$$

For a PMT, the current measured at the anode is the result of the multiplication of electrons emitted at the cathode, the number of which follows a Poisson random process. Here the mean number of electrons ($\overline{N}$) detected was considered, with N being the number of electrons at the cathode within a time period of Δt:

$$\overline{N} = \frac{I_{Cath}\Delta t}{e}, \tag{11}$$

where:

$$I_{Cath} = 2\pi S(L_{AC} + L_{DC})hfE_{Cath} \tag{12}$$

is the cathode current, e is the electron charge, L_{DC} is the unmodulated surface radiance, $L_{AC} = mL_{DC}$, m is the modulation depth, and E_{Cath} is the cathode radiance sensitivity.

The shot noise X can be expressed as:

$$X = N - \overline{N}, \tag{13}$$

the noise current at the anode is:

$$I_{Ano} = \frac{XeG}{\Delta t}, \tag{14}$$

where G is the PMT gain. The noise related to the voltage output from the transimpedance amplifier is:

$$V = I_{Ano}RM. \tag{15}$$

Thus the variance of the noise voltage is:

$$\sigma_V^2 = (\frac{eGRM}{\Delta t})^2\sigma_X^2, \tag{16}$$

where $\sigma_X^2 = \sigma_N^2 = \overline{N}$ according to the property of Poisson process.

Following Parseval's theory the total noise power equals twice the variance of the noise voltage, thus the output noise power due to signal is:

$$P_{ns} = 2\sigma_V^2. \tag{17}$$

The calculations are based on the assumption that a lock-in amplifier is used in detection. If it is supposed for a time window of Δt the bandwidth of the lock-in amplifier is given by $B = \frac{1}{2\Delta t}$, the bandwidth of the system is B as well. The output noise power due to signal can thus be expressed as:

$$P_{ns} = (2\sqrt{eI_{Cath}B}GRM)^2. \quad (18)$$

3.3 Simulated experiment

The simulation experiment was based on a simplified version of an experimental system used in previous studies of USMLT performed in our laboratory using a chemi-luminescent source [12]. Here, the tissue phantom was modelled as a rectangular slab (55 mm × 55 mm × 15 mm) containing a cylindrical bioluminescent source (1 mm diameter, 5 mm height) in the centre of the slab (see Figure 1). The detection system was modelled as a PMT and aperture which were approximated as a circular disk detector (8 mm) located on the surface of the tissue phantom. The mesh generation tool in NIRFAST was then used to discretise the tissue phantom slab and cylindrical bioluminescent source into tetrahedral elements with average edge lengths of 0.2 mm and 0.3 mm using the Delaunay Triangulation method. The circular detector was discretised into triangles of average edge length of 0.2 mm using the same tool. These element sizes were chosen as they are sufficiently small to confer numerical stability and accuracy to the diffusion computations without being computationally expensive. The vertices of the Delaunay Triangulation were used as point sources and point detectors forming the source and detector respectively.

The US field was considered to be generated by a focussed US transducer with the focal zone being approximated as a thin cylinder (2 mm diameter, 18 mm long). Only the US field in this focal zone was considered in the simulation where it was assumed to propagate without attenuation in a linear manner as a plane wave with stratified pressure amplitude variation along the long axis of the cylinder.

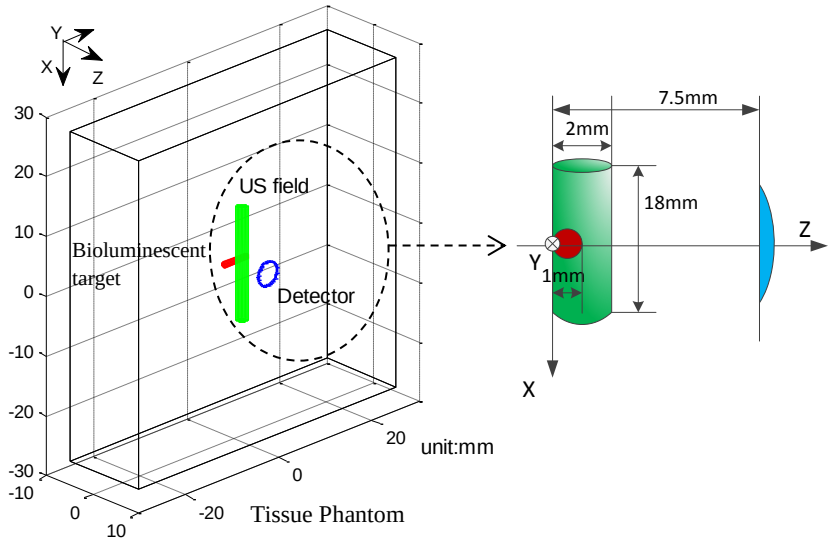

Figure 1 Simulated experimental setup based on a simplified version of the system used in [12] with the tissue phantom being was modelled as a rectangular slab (55 mm × 55 mm × 15 mm) containing a cylindrical bioluminescent source (1 mm diameter, 5 mm height) at a depth of z = 0.5 mm. The US focal zone (green) was simplified as a 2 mm diameter, 18 mm long cylinder and the detector (blue) as a disk located at z = 7.5 mm.

The parameters used in simulations were based on literature values of the optical and physical properties observed in biological tissue [21] and luciferase [19] as listed in Table 1.

adiabatic piezooptical coefficient $\partial n/\partial p$ [18]	1.466×10^{-10} m^{2}N^{-1}	quantum yield QY [19]	0.48 photons per molecule
medium acoustic velocity v_a	1500 m s^{-1}	catalytic constant k_{cat} [19]	3×10^{-2} s^{-1}
medium density ρ_0	1000 kg m^{-3}	C_m ($C_0 = \frac{C_m N_A}{kDa}$) [22]	20 mg ml^{-1}
equilibrium refractive index n_0	1.4	compressibility of medium β_a	4.44×10^{-10} Pa^{-1}
equilibrium reduced scattering coefficient μ_{s0}'	1 mm^{-1}	molar mass of luciferase kDa [23]	62 kg mol^{-1}
equilibrium absorption coefficient μ_{a0}	0.02 mm^{-1}	radius of luciferase	3 nm
fluid kinematic viscosity γ	10^{-6} m^{2}s^{-1}	temperature	293 K

Table 1 Parameters used to simulate the tissue phantom and bioluminescence source, values taken from the literature.

Calculation of the SNR in the simulated experiment were based on the parameters of instrumentation used in previous experimental studies [12]. Table 2 shows values taken from the datasheets of a Hamamatsu H5783-20 PMT and Stanford Instruments SR445A transimpedance amplifier. The simulated radiance emitted at the surface of the mouse was based on literature values

from BLT which was found to lie in the range of 10^6 photons $s^{-1}\,cm^{-2}\,sr^{-1}$ to 10^{11} photons $s^{-1}\,cm^{-2}\,sr^{-1}$ [24, 25].

PMT anode radiance sensitivity E_{Ano}	3.9×10^4 A W^{-1}
PMT cathode radiance sensitivity E_{cath}	78 mA W^{-1}
PMT gain G	4×10^5
input impedance of transimpedance amplifier R	500 Ω
gain of transimpedance amplifier M	5
light wavelength λ	650 nm
lock-in bandwidth B	0.1 Hz

Table 2 Parameters used in SNR calculations based on instrument datasheet and literature values of bioluminescent sources.

4 RESULTS AND DISCUSSION

4.1 Ultrasound modulation of sample optical properties and luciferase concentration

The US induced changes in the reduced optical scattering coefficient, optical absorption coefficient, refractive index, and luciferase concentration dependent bioluminescence emission intensity relative to their equilibrium values were investigated as a function of US pressure using eq. (3) and eq. (7). The applied US field is obtained using eq. (2) and it is over a medically relevant pressure range up to 10 MPa and with an arbitrary frequency of 1 MHz. Figure 2 shows these relative changes of $\Delta\mu_s'/\mu_{s0}', \Delta\mu_a/\mu_{a0}, \Delta n/n_0$ and $\Delta q/q_0$. Results are shown for the pressure maximum in the US cycle which is frequency independent. Over the pressure range considered, a linear increase in the parameter change is seen with pressure. This relationship is clear from inspection of eq. (3) which describes the optical properties of the tissue phantom. The absolute value and rate of change for $\Delta n/n_0$ was the lowest of these parameters which corresponds to the smallest constant in eq. (3a). The change in $\Delta q/q_0$ with pressure from eq. (7) is predicted to be proportional to the applied US pressure as well and it undergoes the greatest change.

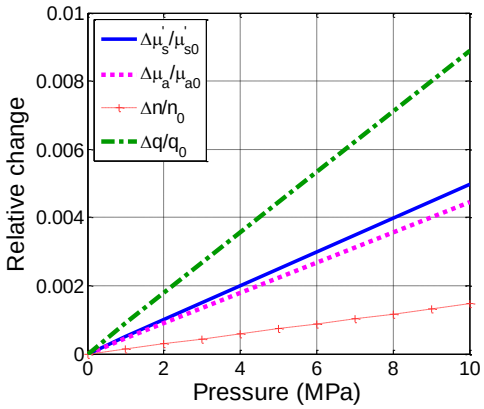

Figure 2 Effect of US pressure (f = 1 MHz) on the relative change in the reduced optical scattering coefficient, optical absorption coefficient, refractive index, and concentration of the bioluminescent target, denoted as $\boldsymbol{\Delta\mu_s'/\mu_{s0}'}$, $\boldsymbol{\Delta\mu_a/\mu_{a0}}$, $\boldsymbol{\Delta n/n_0}$ and $\boldsymbol{\Delta q/q_0}$respectively.

The corresponding changes in modulation depth of the detected signal arising individually from $\Delta\mu_s'/\mu_{s0}'$, $\Delta\mu_a/\mu_{a0}$, $\Delta n/n_0$ and $\Delta q/q_0$ over the 0 MPa to 10 MPa pressure range studied in Figure 2 were also calculated. Figure 3 shows the parameter with the greatest effect on modulation depth is the change in the bioluminescence emission intensity. Figure 3 also shows a linear increase in the modulation depth with US pressure for all four parameters studied. This linear relationship between modulation depth and US pressure is in agreement with the analytic solution obtained by Yuan *et al* [20] and the recent experimental results from Jarrett [26] that demonstrated this for the case of a fluorescent source and an LED source respectively. Although all parameters studied show a linear trend with pressure, their absolute values and rates of change vary considerably. In fact the bioluminescence intensity due to the US induced change of luciferase concentration (Figure 3 (d)) is approximately two orders of magnitude greater than that caused by changes in the reduced scattering coefficient (Figure 3 (a)) and absorption coefficient (Figure 3 (b)) and of the order of 10^5 times higher than that related to changes in the refractive index (Figure 3 (c)). A modulation depth of 3.6×10^{-4} (AC/DC = 3.6 μV/10 mV) was obtained from our previous chemi-luminescence experimental result at a phantom with μ_s = 0.21 mm^{-1} and μ_a = 0.00005 mm^{-1} [3]. The US frequency and peak pressure used were 1 MHZ and 0.42 MPa respectively. Here in this paper the modulation depth at the same frequency, pressure and optical properties was calculated to be 2.1×10^{-4}, which is quite close to the previously measured value. The difference of the significand might be due to the measurements errors and simulation assumptions (e.g. perfect focused US). Of note also is the modulation depth magnitude for the case of bioluminescence is comparable to experimental [4] and theoretically predicted results [5] for fluorescence.

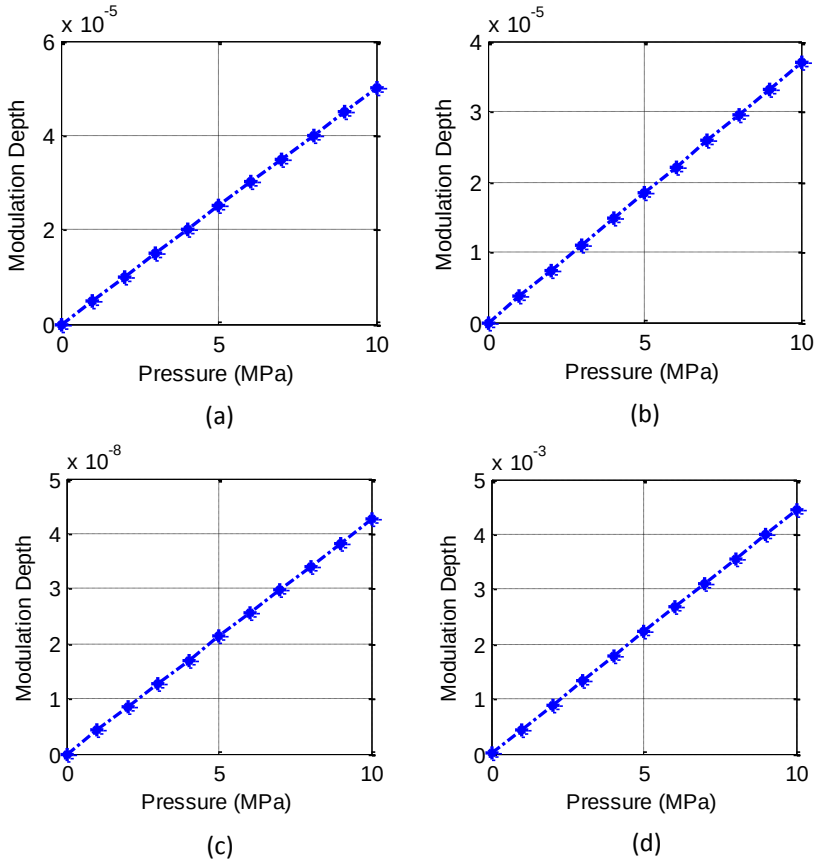

Figure 3 Change in modulation depth arising individually from $\boldsymbol{\Delta\mu_s'}$ (a), $\boldsymbol{\Delta\mu_a}$ (b), $\boldsymbol{\Delta n}$ (c) and $\boldsymbol{\Delta q}$ (d) with respect to maximum US pressure.

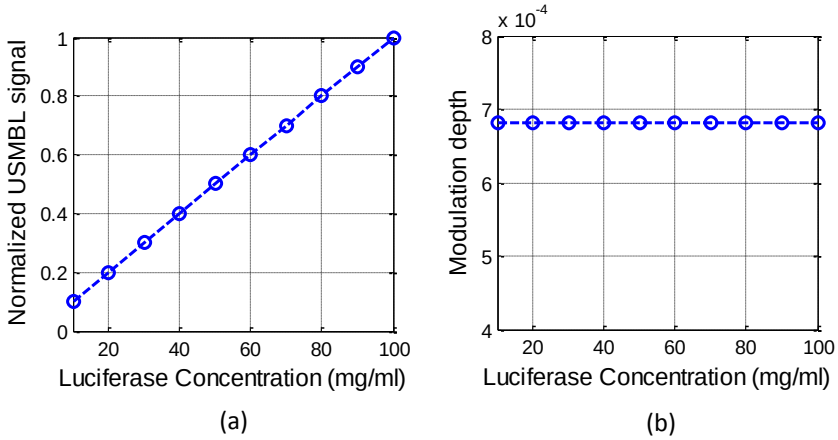

Figure 4 Normalised USMBL signal (a) and modulation depth (b) as a function of luciferase concentration.

The dominance of luciferase concentration dependent changes in bioluminescence intensity on the modulation depth were further investigated by studying the affect luciferase concentration has on the ultrasound modulated signal and modulation depth over a biologically relevant concentration range of 10 mg ml^{-1} to 100 mg ml^{-1}. Figure 4 shows the results of these calculations. Here the normalised ultrasound modulated signal is shown to investigate the trend with concentration which was found to vary with the concentration linearly. This linear relationship of modulated signal with source concentration is consistent with the expression (18) derived in [27]. It should also be noted that in [28] the US modulated fluorescence signal was observed to only increase when the fluorophore concentration is low and it will decrease in the high concentration region. This is due to the 'inner filter effect', in which the excitation light is mostly absorbed by the fluorescent molecules near the light input region, and the fluorescence emission is reabsorbed by the fluorophores along the light transmission path in an optically dense solution [29]. However, the process of generating bioluminescence does not require excitation light for light emission thus no 'inner filter effect' exists for USMBLT. This is an advantage of USMBLT when the USMBL signal is used to quantify the luciferase concentration because the relationship is much simpler. The modulation depth is invariant with luciferase concentration as shown in Figure 4 (b) because the modulated bioluminescence signal and unmodulated signal have the same trend with luciferase concentration.

The spatial variation of US induced changes in $\boldsymbol{\Delta q/q_0}$ and the corresponding modulation depths detected as US propagates through the focal zone were studied. These variations are a result of the sinusoidal nature of the modelled US wave which produces a spatial and temporal variation in pressure along the focal zone, both of which are a function of the applied US frequency. Figure 5 shows the variation in $\boldsymbol{\Delta q/q_0}$ caused by a 0.75 MHz, 1 MPa ultrasound wave along the length of the bioluminescence source (x direction) over a time frame corresponding to one period of wave oscillation.

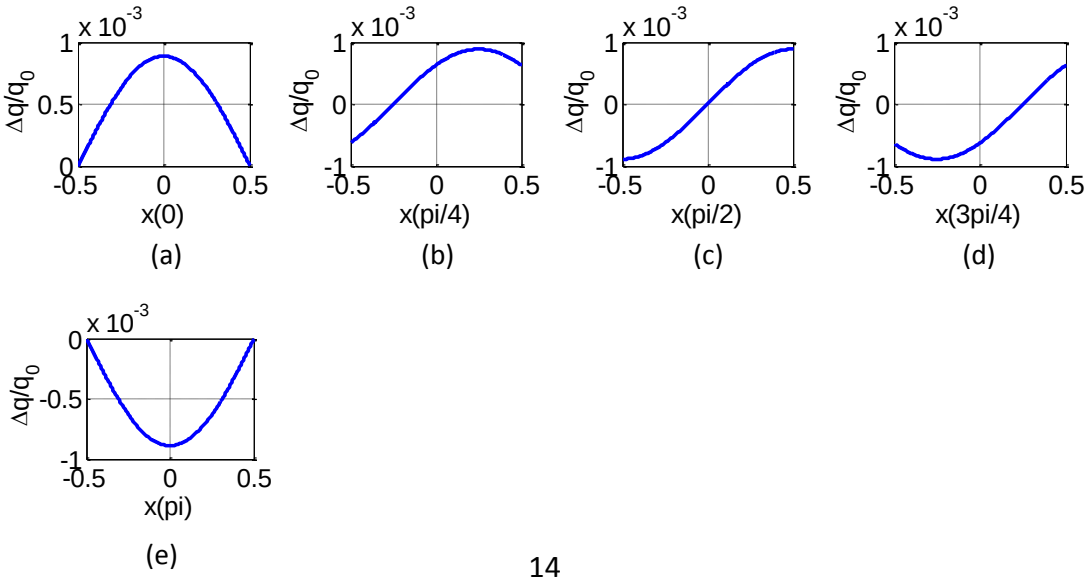

Figure 5 Oscillation of $\boldsymbol{\Delta q/q_0}$ over one US period at a frequency of 0.75 MHz. The relative phase of the US is labelled on the x axis.

The observed spatial variation in $\boldsymbol{\Delta q/q_0}$ as the sound propagates is a result of the changing US pressure distribution and affects the modulation depth of the detected signal. The modulation depth for US frequencies of 0.75 MHz, 1.5 MHz and 2.25 MHz was also calculated. The pressure distributions set up by each frequency will vary as a result of their differing wavelengths and their size relative to that of the bioluminescence source. Here the 1 mm diameter source simulated corresponds to distances equal to λ/2, λ, 3λ /2 respectively of the three frequencies studied. The resulting variation in modulation depth for these three conditions was calculated and is shown in Figure 6. It should be noted that Figure 6 includes US induced changes in the reduced optical scattering coefficient, optical absorption coefficient and refractive index but these are dominated by changes in concentration.

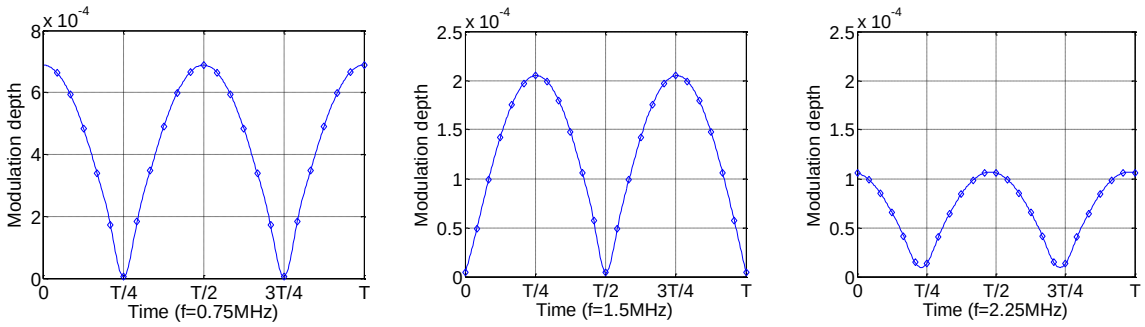

Figure 6 Oscillation of modulation depth of the detected signal over one US period for frequencies of 0.75 MHz (a), 1.5 MHz (b) and 2.25 MHz (c).

The modulation depth is shown in Figure 6 (a) to be a maximum when the phase is 0, at which time the relative change of source intensity is even symmetrical, as shown in Figure 5 (a). The oscillation of the modulation depth is due to the summation of USMBL signals originating from each layer of the source region along the US transmission direction at the detector. When the US pressure distribution is even symmetrical to the centre axis of the cylindrical source, the USMBL signals from two symmetrical layers of the source are in phase and sum constructively at the detector so the modulation depth is the highest. When the US pressure distribution is odd symmetrical to the centre axis, the USMBL signals from the two symmetrical layers of the source are out of phase and sum destructively at the detector so the modulation depth is the lowest. It should be noted that when the phase sum or absolute difference is π, the modulation depths are the same. This is because the pressure distributions within the source region at these conditions are either odd symmetrical or even symmetrical with each other (e.g. (b) and (d)) in Figure 5. Since modulation depth is an absolute value, its frequency is twice that of the US. A similar trend is observed in Figures 6 (b) and

(c) with the modulation depth varying at twice the US frequency. Interestingly the maximum modulation depth is found to decrease with increase in frequency over the range studied. It is thought that this observation is related to the size of the bioluminescence source and the ultrasound frequency as has been observed in studies of ultrasound modulated fluorescence tomography [8].

It should be noted that these findings are based on simulations of a simplified experimental situation in which the tissue phantom is considered to be homogenous, unlike the case of real biological tissue. In addition, US propagation to the focal zone is not modelled and only the pressure at the fundamental frequency is considered in this paper. It is assumed that there is no attenuation within the focal zone. These assumptions will result in the modelled US field distribution differing from the experimental situation on account of US non-linear propagation, absorption, scattering, and beam divergence. All the speed related parameters in section 2 would also become functions of position and time instead of constants. However, the magnitude of the calculated modulation depth should still be the same because the fundamental component of US would always dominant. Nevertheless, further work will involve incorporation of these effects into the NIRFAST software tool through the use of an acoustic toolbox such as k-Wave [30] to model pressure distribution more realistically.

4.2 SNR analysis of *in vivo* detection

The effect of PMT diameter, surface radiance of bioluminescence and modulation depth on the SNR of USMBLT system were analysed based on the method described in section 2. Figure 7 shows the SNR calculated for six different surface radiances ($10^6, 10^7, 10^8, 10^9, 10^{10}$, and 10^{11} photons $s^{-1}\,cm^{-2}\,sr^{-1}$) as a function of PMT diameter with an RMS modulation depth of 9.6×10^{-4} (Figure 7 (a)) and as a function of modulation depth for a fixed PMT diameter of 8 mm (Figure 7 (b)). The contribution of the ambient light and the dark current to the noise power were estimated based on a noise voltage level of 0.4 μV_{rms}, as detected in a previous experiment [12].

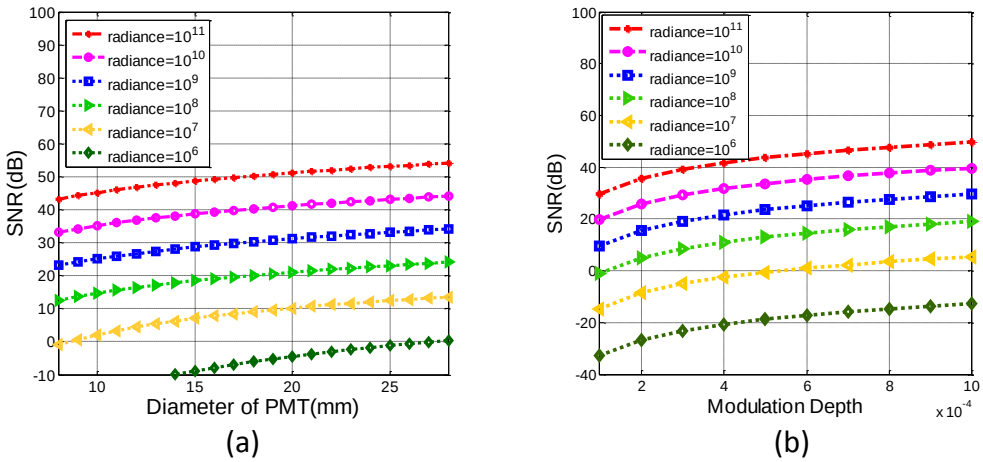

Figure 7 SNR simulation for USMBLT experiments for different surface radiance as a function of PMT diameter, modulation depth = 9.6×10^{-4} (a); and as a function of modulation depth, PMT diameter = 8 mm (b).

The feasibility of applying USMBLT to pre-clinical imaging is contingent on detection of modulated optical signals within the noise limits of current detector technologies. Results in Figure 7 are based on calculations for a mouse model with detector capabilities matching that of a PMT used in previous experimental studies (Hamamatsu H5783-20). Inspection of Figure 7 (a) shows SNRs achieved with radiances ranging from 10^6 photons $s^{-1}\,cm^{-2}\,sr^{-1}$ to 10^7 photons $s^{-1}\,cm^{-2}\,sr^{-1}$ fall below the noise level of the simulated detector. However, for radiances above 10^7 photons $s^{-1}\,cm^{-2}\,sr^{-1}$ the SNRs are comfortably detectable within the limits of the detector modelled in [12]. Apart from changing the radiance, the SNR can also be improved by increasing the PMT diameter as seen in Figure 7 (a) and the modulation depth as shown in Figure 7 (b). It is noted that the nonlinear relationship of SNR with respect to radiance was caused by the 0.4 μV_{rms} noise voltage level from dark current and ambient light.

Overall there are good prospects for the application of USMBLT in pre-clinical imaging. Besides, considerable effort has been directed to establish novel luciferases that can exert a brighter, stable, and red-shifted bioluminescence by mutation [31, 32], DNA optimization [33] or bioluminescence resonance energy transfer with fluorescent proteins [34]. A novel luciferase NLuc has also been established that can emit approximately 100-fold brighter and more stable bioluminescence than the gene firefly luciferase (Fluc) studied here [35]. Such signal improvement will lead to greater SNRs and enhance the quality of USMBLT images. Other strategies to improve the modulated optical signal relate to the use of ultrasound microbubble contrast agents that have high compressibility and as such have the capability to increase the change in the bioluminescent source intensity as indicated by eq. (7) [7].

5 CONCLUSION

In this work numerical simulations were carried out to investigate the mechanisms dominant in generation of USMBL signals using the NIRFAST software tool. Simulations were based on the optical and physical properties of a mouse model and detection capabilities of instrumentation used in previous experimental work. Results demonstrate that the dominant effect in generation of USMBL is ultrasound induced variation in luciferase concentration. This effect was determined to be approximately two orders of magnitude greater than that caused by changes in the reduced scattering coefficient and absorption coefficient and of the order of 10^5 times higher than that related to changes in the refractive index. These findings make it clear that to improve the

compressibility of the luciferase-luciferin solution and thus the variation of its concentration with US is the major way to improve the modulation depth.

The effect of US frequency on modulation depth was also studied. Depending on the distribution of the sinusoidal pressure along the US transmission direction, the USMBL signals can sum either constructively or destructively at the detector, which results in an oscillation of the modulation depth over time. The results here predict the modulation depth varies at twice the US frequency and its absolute value is a function of the US wavelength relative to the bioluminescence source size.

The SNR analysis results confirm the feasibility of applying USMBLT in preclinical imaging of mice to improve the spatial resolution of BLI. It was determined that for surface radiances above approximately 10^7 photons s^{-1} cm^{-2} sr^{-1} the corresponding SNRs are detectable with devices currently used in [12]. The development of novel luciferases that can exert bioluminescence above such radiance level will also make the application highly potential. The measured USMBL signal can provide valuable data for BLI reconstruction to make the reverse problem less ill-conditioned.

Acknowledgment

M. Mather is supported by the Engineering and Physical Sciences Research Council UK (EP/J001953/1). Q. Zhang is funded by the China Scholarship Council. The research is also supported by the National Centre for the Replacement, Refinement and Reduction of Animals in Research (NC/L00187X/1).

References

1. S.M. Marques et al., "*Firefly bioluminescence: A mechanistic approach of luciferase catalyzed reactions,"* IUBMB Life, 61(1), 6-17 (2009).
2. A. Roda, and M. Guardigli, "*Analytical chemiluminescence and bioluminescence: latest achievements and new horizons,"* Anal. Bioanal. Chem. 402(1), 69-76 (2012).
3. T. J. Snoeks et al., "*'In vivo' optical approaches to angiogenesis imaging,"* Angiogenesis. 13(2), 135-147 (2010).
4. H. Dehghani et al., "*Spectrally resolved bioluminescence optical tomography,"* Opt. Lett.. 31(3), 365-367 (2006).
5. P. Beard, "*Biomedical photoacoustic imaging,"* Interface Focus. 1(4), 602-631(2011).
6. D. S. Elson et al., "*Ultrasound-mediated optical tomography: a review of current methods,"* Interface Focus. 1(4), 632-648 (2011).
7. B. Yuan et al., "*Microbubble-enhanced ultrasound-modulated fluorescence in a turbid medium,"* Appl. Phys. Lett. 95(18), 181113 (2009).
8. N. T. Huynh et al., "*Effect of object size and acoustic wavelength on pulsed ultrasound modulated fluorescence signals,"* J. Biomed. Opt. 17(7), 076008 (2012).
9. M. Kobayashi et al., "*Fluorescence tomography in turbid media based on acousto-optic modulation imaging,"* Appl. Phys. Lett. 89(18), 181102 (2006).
10. H. Ruan, "*Pulsed Ultrasound Modulated Optical Tomography with Parallel Speckle Detection,"* PhD thesis, Univ.Nottingham (2012).
11. Y. Liu et al., "*Effect of fluorescent particle size on the modulation efficiency of ultrasound-modulated fluorescence,"* Int. J. Opt., 260709 (2012).
12. N. T. Huynh et al., "*Ultrasound modulated imaging of luminescence generated within a scattering medium,"* J. Biomed. Opt. 18(2), 20505 (2013).

13. G. Bal and J.C. Schotland, "*Ultrasound-modulated bioluminescence tomography,*" Phys. Rev. E, 89(3) (2014).
14. H. Dehghani et al., "*Near infrared optical tomography using NIRFAST: Algorithm for numerical model and image reconstruction,*" Commun. Numer. Methods Eng. 25(6), 711-732 (2008).
15. J.A. Guggenheim et al., "*Quantitative surface radiance mapping using multiview images of light-emitting turbid media,*" J. Opt. Soc. Am. A. 30(12), 2572-2584 (2013).
16. W. D. Jr, "*Ultrasound–biophysics mechanisms,*" Prog. Biophys. Mol. Bio. 93(1–3), 212-255 (2007).
17. Q. Liu et al., "*Modeling of nonphase mechanisms in ultrasonic modulation of light propagation,*" Appl. Opt. 47(20), 3619-3630 (2008).
18. L. V. Wang, "*Mechanisms of ultrasonic modulation of multiply scattered coherent light: An analytic model,*" Phys. Rev. Lett. 87(4), 043903 (2001).
19. K. Niwa et al., "*Quantum yields and kinetics of the firefly bioluminescence reaction of beetle luciferases,*" Photochem. Photobiol. 86(5), 1046-1049 (2010).
20. B. Yuan et al, "*Mechanisms of the ultrasonic modulation of fluorescence in turbid media,*" J. Appl. Phys. 104(10), 103102 (2008).
21. J. L. Sandell and T.C. Zhu, "*A review of in-vivo optical properties of human tissues and its impact on PDT,*" J. Biophotonics. 4(11-12), 773-787 (2011).
22. M. Barry et al., "*Imaging Luciferase-Expressing Viruses*," Oncolytic Viruses, Humana Press. 79-87(2012).
23. E. Conti et al., "*Crystal structure of firefly luciferase throws light on a superfamily of adenylate-forming enzymes,*" Structure, 4(3), 287-298 (1996).
24. D. M. Barrett et al., "*Noninvasive bioluminescent imaging of primary patient acute lymphoblastic leukemia: a strategy for preclinical modeling,*" Blood, 118(15), 112-117, (2011).
25. H. Zhao et al., "*Emission spectra of bioluminescent reporters and interaction with mammalian tissue determine the sensitivity of detection in vivo,*" J. Biomed. Opt. 10(4), 041210 (2005).
26. C.W. Jarrett et al., "*Detection of a Novel Mechanism of Acousto-Optic Modulation of Incoherent Light,*" PLoS ONE. 9(8), e104268 (2014).
27. T. Duc et al., "*Study on mechanism of ultrasonic fluorescence modulation in light scattering medium based on diffusion approximation with varying refractive index,*" Optical Review. 19(3), 159-166 (2012).
28. B. Yuan and Y. Liu, "*Ultrasound-modulated fluorescence from rhodamine B aqueous solution,*" J. Biomed. Opt. 15(2), 021321 (2010).
29. J.R. Lakowicz, "*Principles of Fluorescence Spectroscopy", 3rd edition,* Springer US. (2006).
30. B.E. Treeby and B.T. Cox, "*k-Wave: MATLAB toolbox for the simulation and reconstruction of photoacoustic wave fields,*" J. Biomed. Opt. 15(2), 021314 (2010).
31. H. Fujii et al., "*Increase in bioluminescence intensity of firefly luciferase using genetic modification,*" Anal. Biochem. 366(2), 131-136 (2007).
32. K. Noda et al., "*Single bacterial cell detection using a mutant luciferase,*" Biotechnol. Lett. 30(6), 1051-1054 (2008).
33. Y. Nakajima et al., "*Enhanced beetle luciferase for high-resolution bioluminescence imaging,*" PLoS One. 5(4), 10011 (2010).
34. K. Saito et al., "*Luminescent proteins for high-speed single-cell and whole-body imaging,*" Nat. Commun. 3, 1262 (2012).
35. T. Ozawa et al., "*Advances in fluorescence and bioluminescence imaging,*" Anal. Chem. 85(2), 590-609 (2013).